

# Earth and Space Science

## RESEARCH ARTICLE

10.1029/2020EA001105

### Key Points:

- Relative roles of SSTs of Tropical Pacific and Indian Ocean and Eurasian snow on the Indian and Korean monsoons have been examined at 40 km resolution using GME
- A negative (positive) relationship between the Western (Eastern) Eurasian snow depth and ISMR has been found
- A positive(negative) relationship between the Western(Eastern) Eurasian snow depth and Korean monsoon rainfall has been observed

### Supporting Information:

- Supporting Information S1

### Correspondence to:

S. K. Panda,  
subrat.atmos@curaj.ac.in

### Citation:

Panda, S. K., Hong, M.-J., Dash, S. K., Oh, J.-H., & Pattnayak, K. C. (2020). Relative roles of Eurasian snow depth and sea surface temperature in Indian and Korean summer monsoons based on GME model simulations. *Earth and Space Science*, 7, e2020EA001105. <https://doi.org/10.1029/2020EA001105>

Received 23 JAN 2020

Accepted 23 APR 2020

Accepted article online 18 MAY 2020

### Author Contributions:

**Conceptualization:** S. K. Panda, S. K. Dash, Jai-Ho Oh




**Formal analysis:** Mi-Jin Hong, Jai-Ho Oh, K. C. Pattnayak

**Writing – review & editing:** S. K. Panda

©2020. The Authors.

This is an open access article under the terms of the Creative Commons Attribution License, which permits use, distribution and reproduction in any medium, provided the original work is properly cited.

## Relative Roles of Eurasian Snow Depth and Sea Surface Temperature in Indian and Korean Summer Monsoons Based on GME Model Simulations

S. K. Panda<sup>1,2</sup> , Mi-Jin Hong<sup>3</sup>, S. K. Dash<sup>1</sup>, Jai-Ho Oh<sup>3</sup> , and K. C. Pattnayak<sup>1,4</sup> 

<sup>1</sup>Centre for Atmospheric Sciences, Indian Institute of Technology Delhi, New Delhi, India, <sup>2</sup>Department of Atmospheric Science, School of Earth Sciences, Central University of Rajasthan, Kishangarh, India, <sup>3</sup>Department of Environmental Atmospheric Sciences, Pukyong National University, Busan, South Korea, <sup>4</sup>School of Earth and Environment, University of Leeds, Leeds, UK

**Abstract** Indian Summer Monsoon (ISM) and East Asian Summer Monsoon (EASM) are the most important weather systems in India and Korea respectively. The interannual variations of ISM and EASM largely depend on the anomalies of sea surface temperatures (SSTs) of Tropical Equatorial Pacific and Indian Ocean and also on the Eurasian Snow Depth/Cover. In this study, the relative roles of these two most important surface boundary conditions on the Indian and Korean monsoons have been examined using the high resolution (40 km) global numerical weather prediction model of German Weather Service (GME). Four sets of experiments were carried out by varying the climatological and observed values of SSTs and snow. This study shows that there is a negative (positive) relationship between the Western (Eastern) Eurasian snow depth and ISMR, whereas a positive (negative) relationship between the Western (Eastern) Eurasian snow depth and Korean monsoon rainfall has been observed. Results show that when observed SST and snow are prescribed to the model as boundary conditions, the simulated winds and rainfall are close to the NCEP/NCAR reanalyzed winds and GPCP rainfall, respectively. This study reveals that the model simulated summer monsoons in Indian and Korean domains are not good enough unless an observed Eurasian snow is prescribed in addition to the observed SST.

## 1. Introduction

The Asian monsoon is broadly classified into two subsystems, namely, the Indian summer monsoon and East Asian Summer Monsoon (EASM) (Yihui & Chan, 2005). Indian monsoon is the lifeline of India, and the economy of the country mostly depends upon the monsoon rain. Most of the rainfall in India occurs during June, July, August, and September, which is referred to as the Indian Summer Monsoon Rainfall (ISMR) or southwest monsoon. The East Asian summer monsoon system is dominant mainly over China, Japan, and Korea. The most significant weather phenomenon during the summer season in Korea is the quasi-stationary front extending from south China to southern Japan. This front is called “Changma” in Korea. The Changma season gets a large portion of the annual rainfall, and most of the droughts and floods over the Korean peninsula occur in this season (Oh et al., 1997). About 50–60% of the annual rainfall over this region occurs during northern summer. They are characterized by frontal rain systems between the two major anticyclonic circulations over the subtropics and the polar regions. The interannual variability of ISMR is affected by anomalous states of lower boundary conditions such as sea surface temperature (SST), snow cover/depth, and soil moisture (Charney & Shukla, 1981). One of the major forcings for the interannual variability of ISMR is the SST distribution in the Tropical Pacific and Indian Ocean. Snow has been considered to be a critical component of the climate system and has a strong influence on the continental surface energy budget (Cess et al., 1991; Cohen & Rind, 1991; Meehl & Washington, 1990; Randall et al., 1994). During the winter season, more than 60% of the Eurasian continent is covered with snow (Morinaga et al., 2003), which affects local and large-scale atmospheric circulation and hydrological processes by changing the process of energy and water transfer between the land and atmosphere.

Several observational and modeling studies indicate that the strength of the Indian summer monsoon is inversely related to the Eurasian snow extent and depth in the preceding season. In the past, a number of sensitivity experiments have been conducted by using General Circulation Models (GCMs) to study the

effect of winter/spring Eurasian snow anomalies on the subsequent summer monsoon (Barnett et al., 1989; Dash et al., 2006; Ferranti & Molteni, 1999; Karri et al., 2018; Ose, 1996; Panda et al., 2016; Tiwari et al., 2016; Vernekar et al., 1995). To confirm the inverse snow-ISMR relationship and to examine the influence of Eurasian snow depth on the Asian summer monsoon circulation, Dash et al. (2006) conducted sensitivity experiments using GCM of Indian Institute of Technology Delhi (IITD) (2005). Earlier, Blanford (1884) had hypothesized that varying extent and thickness of the Himalayan snow have a prolonged and large influence on the climatic conditions and weather over the plains of north-west India (Blanford, 1884). The high albedo of the snow and moisture from snow melt work together to reduce land surface heating and thus delay the onset of monsoon and consequently the monsoon rainfall amounts (Bamzai & Shukla, 1999; Douville & Royer, 1996; Kripalani & Kulkarni, 1999; Parthasarathy & Yang, 1995). The effect of Tibetan spring snow on the Indian Summer Monsoon circulation and associated rainfall using RegCM3 has been studied by Shekhar and Dash (2005). Results show that Tibetan snow in April reduces the low-level westerlies and upper level easterlies during subsequent summer monsoon over India. Model simulations show that when 10 cm of snow depth in April is prescribed over Tibet, summer monsoon rainfall in entire India reduces by about 30%.

Mooley and Parthasarathy (1984) examined the relationship between all-India summer monsoon rainfall and SST anomaly over the eastern equatorial Pacific and obtained negative correlation coefficient (Mooley & Parthasarathy, 1984). The seasonal mean monsoon rainfall has been shown, in observational and model studies, to have maximum correlation with the SST of the East Pacific Ocean when the monsoon leads the SST by four to six months (Kirtman & Shukla, 2000). During the past few years, coupled ocean-atmosphere models have also been used to study the relationship between the monsoon and SST anomalies of the Pacific and Indian Oceans. In brief, most of the studies have shown that the tropical Pacific SST is important in modulating the interannual variability of Asian summer monsoon while the role of the Indian Ocean SST remains uncertain. Early atmospheric GCM studies aimed mainly at the response of monsoon to idealized SST forcing in either the Pacific Ocean or the Indian Ocean (Keshavamurty, 1982; Shukla, 1975). In contrast, study by Palmer et al. (1992) has been focused on underlying changes in the monsoon associated with observed SST anomalies (Palmer et al., 1992). Yang (1996) found that more (less) Eurasian winter snow cover occurs during El Niño (La Niña) events and that the usual snow-monsoon links break down during the El Niño episodes (Yang, 1996). Sankar-Rao et al. (1996) also suggested that the snow-monsoon rainfall relationship becomes stronger when partial correlation is used to exclude the El Niño years (Sankar-Rao et al., 1996). Liu and Yanai (2002) showed that the impact of snow cover on the Asian monsoon was seen more clearly once the effects of ENSO were removed (Liu & Yanai, 2002). Fasullo (2004) also supported the snow mechanism (Fasullo, 2004) proposed by Blanford (1884) but agreed that the effect can be overwhelmed by ENSO.

Many studies have also investigated the influence of Eurasian and Tibetan snow on EASM. Yang and Xu (1994) showed that the relationship between Eurasian winter snow cover and summer rainfall in southern and northern China was positively correlated, whereas an inverse relationship was found between Eurasian winter snow and subsequent summer rainfall in western, central, and northeastern China (Yang & Xu, 1994). Liu and Yanai (2002) found that large Eurasian snow cover in spring leads to cooling and a cyclonic circulation anomaly in the lower troposphere over Eurasia, forming a Rossby wave train response and then leading to below-normal EASM rainfall (Liu & Yanai, 2002). Seol and Hong (2009) have suggested that above-normal snowfall over the Tibetan Plateau in May induces weakening of the Tibetan high, which leads to the formation of favorable upper-level circulations accompanying cyclonic circulation anomalies covering the East Asian region in summer with the use of global and regional model (Seol & Hong, 2009). Yim et al. (2010) pointed out that a strong dipole pattern with positive (negative) snow cover anomalies over western Eurasia and negative (positive) snow cover anomalies over eastern Eurasia signifies enhanced (reduced) summer rainfall over East Asia (Yim et al., 2010). Kripalani et al. (2002) also suggested that winter/spring snow depth over western (eastern) Eurasia is negatively (positively) related to KMR (Kripalani et al., 2002). They even developed a multiple linear regression equation to forecast the relationship between snow depth and KMR. However, they pointed out that KMR is not well estimated during the El Niño years.

Although several studies have been conducted on the observational and modeling aspects of the inverse relationship between ISMR and Eurasian snow extent/depth, not much has been studied about KMR. The

relative roles of these two important forcings on both the monsoons have not been examined so far. The purpose of this study is to examine the influence of Eurasian snow depth *visa-a-vis* that of SST on Indian as well as Korean summer monsoons using the same model (i.e., GME) at high resolution. A brief description of the GME model, data used for this study and experimental design are described in section 2. Section 3 discusses relationship between the Eurasian snow depth and Indian and Korean Summer Monsoons based on observations. The model biases in all the experiments have been presented in section 4. Section 5 evaluates the performance of the model in all the four experiments conducted. A comparative study of the results obtained from the sensitivity experiments is made in section 6. Major findings of this paper are summarized in section 7.

## 2. Data and Experimental Design

### 2.1. GME Model and Data Used

The global numerical weather prediction model of German Weather Service (Deutscher Wetterdienst) called GME has been installed at PuKyong National University (PKNU), Busan, South Korea. The name originated from the fact that it replaced the operational Global Model (GM) and the regional model for central Europe (EM). It is a hydrostatic atmospheric GCM with icosahedral-hexagonal grid. Version 2.17 of GME is used in this study. One of the advantages of the icosahedral-hexagonal grid is the avoidance of the so-called pole problem that exists in conventional latitude-longitude grids. The structure of initial and boundary conditions prescribed to GME is extremely well suited for high efficiency on distributed memory parallel computers. The primitive equations are solved using a finite-difference method on a hexagonal icosahedral A-grid. The model has a horizontal resolution of 40 km and 40 hybrid levels in the vertical. Operationally, the model is initialized using a three-dimensional variational data assimilation system (Reitter et al., 2011). Four hydrometeor classes are implemented in the model: cloud ice and water, snow, and rain. They are available as grid-scale parameters. In the operational version of the GME, cloud ice and cloud water are prognostic variables, whereas snow and rain are diagnostic variables. The main prognostic variables of GME are surface pressure, horizontal wind components, temperature, specific contents of water vapor, cloud water and cloud ice, rain, snow, and ozone on 60 model layers in the atmosphere from the surface up to a height of approximately 34 km. In this model, the prognostic equations for horizontal winds, temperature, and surface pressure are solved using semi-implicit Eulerian approach. In the vertical direction, finite difference scheme is applied in a hybrid (sigma pressure) coordinate system to all the prognostic variables (Majewski et al., 2002). In this study, the GME (ni = 192, L40) has been integrated at high resolution such as 40-km corresponding to T511L91 of ECMWF, where  $n_i$  is the number of equal intervals into which each side of the original icosahedral triangles is divided. Here, the number of grid points are 368 X 642 and transform grid uses 900 X 451 grid cells. The model has 40 levels in the vertical with the model top at 10 hPa. Detailed description of the model is given in Majewski et al. (2002).

The initial conditions for the model simulations are obtained from the operational ECMWF analysis (T511L91). The Optimum Interpolated (OI) weekly observed SST gridded data have been obtained from the National Oceanic and Atmospheric Administration (NOAA) (Reynolds et al., 2002). This analysis uses in situ and satellite SST's plus SST's simulated by sea-ice cover. The OI analysis is done over all ocean areas and the Great Lakes. There is no analysis over land. The land values are filled by a Cressman interpolation to produce a complete grid for possible interpolation to other grids. The ocean and land areas are defined by a land sea mask. The snow depth data of ERA-interim from 25 April 1985 to 2004 have been used in the snow analysis and conducting sensitivity experiments. ERA-Interim (Dee et al., 2011) is a global atmospheric reanalysis from 1979 to present. ERA-Interim is produced by the European Centre for Medium-Range Weather Forecasts (ECMWF). It is produced with a 2006 version of the IFS (Cy31r2) and continues to be updated in real time. The model simulated rainfall values have been compared against GPCP (Adler et al., 2003) version 2 and of IMD (Rajeevan & Bhate, 2009) and KMA data sets. GPCPv2 data set consists of monthly means of precipitation derived from satellite and gauge measurements. The GPCP combined precipitation data were developed and computed by the NASA/Goddard Space Flight Center's Laboratory for Atmospheres as a contribution to the GEWEX Global Precipitation Climatology Project. IMD has prepared a very good daily gridded ( $1^\circ \times 1^\circ$ ) rainfall data series, which provides a good source for examining spatial and temporal changes in the past years. IMD has generated daily rainfall at regular  $10 \times 10$  grids over the Indian landmass. Rajeevan and Bhate (2009) and Rajeevan et al. (2005) have discussed the methods of gridded data

preparation in detail. They have considered daily rainfall data of 6,329 stations during the period 1951 to 2004. Out of all the stations at only 1,803 stations minimum of 90% data were available. In their analysis, the interpolation method proposed by Shepard (1968) has been followed. This method is based on the weights calculated from the distance between the stations and the grid points and also the directional effects. The IMD gridded rainfall dataset is being extensively used for many applications in validation of climate and numerical weather prediction models and also for studies on monsoon variability (Dash et al., 2009; Goswami et al., 2006; Panda et al., 2016; Pattanayak et al., 2013; Rajeevan & Bhate, 2009). The NCEP/NCAR reanalyzed winds at 850 and 200 hPa and temperature at 500 hPa are used for the validation of model fields simulated in the sensitivity experiments. The NCEP/NCAR Reanalysis (Kalnay et al., 1996) project used a state-of-the-art analysis/forecast system to perform data assimilation using past data from 1948 to the present. Details of NCEP/NCAR reanalysis are described in Kalnay et al. (1996).

## 2.2. Experimental Design

In this study, GME model has been integrated from 25 April to 30 September in each of the years covering the period 1985 to 2004. Here, daily interpolated weekly-observed values of SST and snow depth are used for conducting four sensitivity experiments. In Exp1, climatological SST and snow are used, and this experiment is considered as the control run. Climatological snow is being replaced by observed snow in Exp2 to study the impact of observed snow in the interannual variability of ISMR and KMR. Exp3 is based on the observed SST and climatological snow. Both observed SST and snow are used in Exp4 to examine the impact of observed surface boundary conditions in the interannual variation of rainfall and circulation features. The snow depth data are prescribed on the starting date of model integration, and afterwards, GME model generates its own snow and utilizes it for subsequent time steps. Thus, GME has interactive snow. The GME has been prescribed observed SST in Exp3 and Exp4 and observed snow in Exp2 and Exp4. The difference between the Exp4 and Exp1 indicates the combined role of observed SST and snow in comparison to that of climatological SST and snow. The difference between the Exp4 and Exp3 is the measure of the impact of observed snow alone in comparison to its climatological values in the presence of observed SSTs. Similarly, the role of observed SST as against climatological SST in the presence of observed snow has been indicated in the difference between the Exp4 and Exp2.

## 3. Relationship Between the Eurasian Snow Depth and Indian and Korean Summer Monsoons Based on Observations

The detailed analysis of the relationship between the Eurasian snow depth and Indian as well as Korean summer monsoons is done in this section. The snow depth values for the period 1985 to 2004 used in this study are obtained from the European Centre for Medium-Range Weather Forecasts (ECMWF) Re-Analysis dataset (ERA-Interim) (Dee et al., 2011). The observed rainfall values for the above period have been obtained from Global Precipitation Climatology Project (GPCP) (Adler et al., 2003) data set for evaluating the GME model simulated rainfall.

December, January, and February (DJF) seasonal mean snow depth averaged over the period 1985 to 2004 has been depicted in Figure 1a. There is a large variation of snow depth in the range of 15–50 cm over the Russia region. The snow variation is more over the high-latitudes, and it spreads southwards up to 50°N (Figure 1a). The annual cycle of the snow depth over the Western and Eastern Eurasia regions (as identified by Kripalani et al., 2002) and over the whole Eurasia as done by Dash et al. (2004) is shown in Figures 2a–2c. This figure depicts that snow depth is maximum in the months of February and March over the whole of Eurasia. The snow depth starts with 1 cm in October and increases up to its highest value of 20 cm in February over the Western Eurasia (Figure 2b) whereas it varied from 1 cm in September to 41 cm in March over the Eastern Eurasia (Figure 2c). The standard deviation of snow depth increases with increasing depth for each month over Western Eurasia, but for Eastern Eurasia, it remains constant.

Figure 1b shows that snow depth anomalies over West Eurasia (region A of Figure 1a) in December of the previous year, and January and February of the current year have a negative Correlation Coefficient (CC) with the following ISMR. The Partial Correlation Coefficient (PCC) between standardized DJF snow depth anomalies over the boxes A, B, and C (Figure 1b) and following ISMR anomalies are  $-0.55$  (95% significant),  $0.45$  (95% significant), and  $0.30$  (not significant), respectively. On the other hand, DJF snow depth anomalies over East Eurasia (region B of Figure 1a) have positive CC with subsequent ISMR. These results confirm the

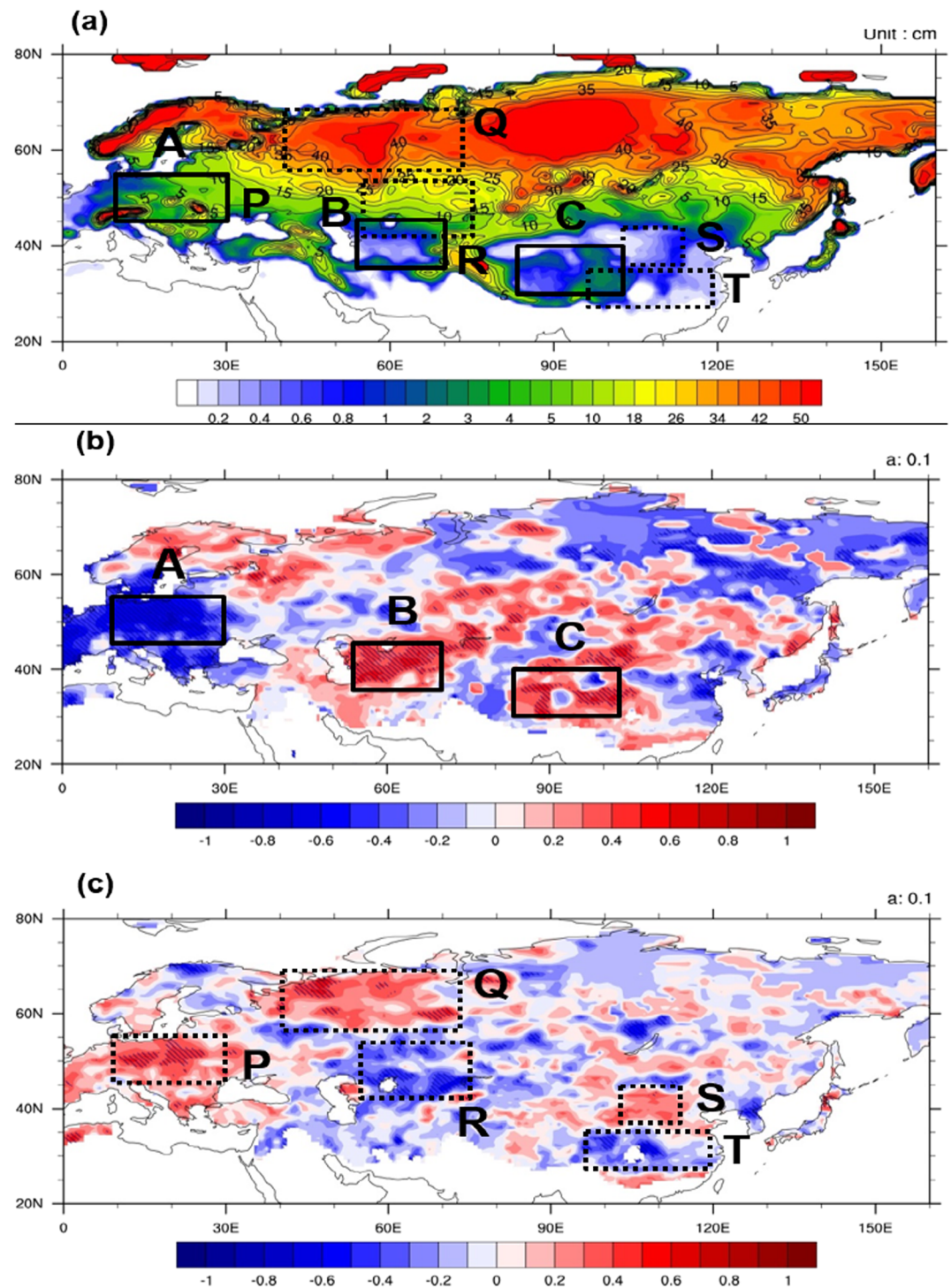


**Figure 1.** DJF snow depth (cm) climatology (a) during the period 1985 to 2004, correlation coefficients (CCs) between DJF Eurasian snow depth anomalies with the following (b) ISMR and (c) KMR. The boxes A, B, and C with solid boundary lines represent the areas over which CCs between DJF Eurasian snow depth anomalies with the following ISMR are significant at 95% confidence level. The boxes P, Q, R, S, and T with dotted boundary lines represent similar areas in case of KMR. It may be noted that regions P and A merge together in (a).

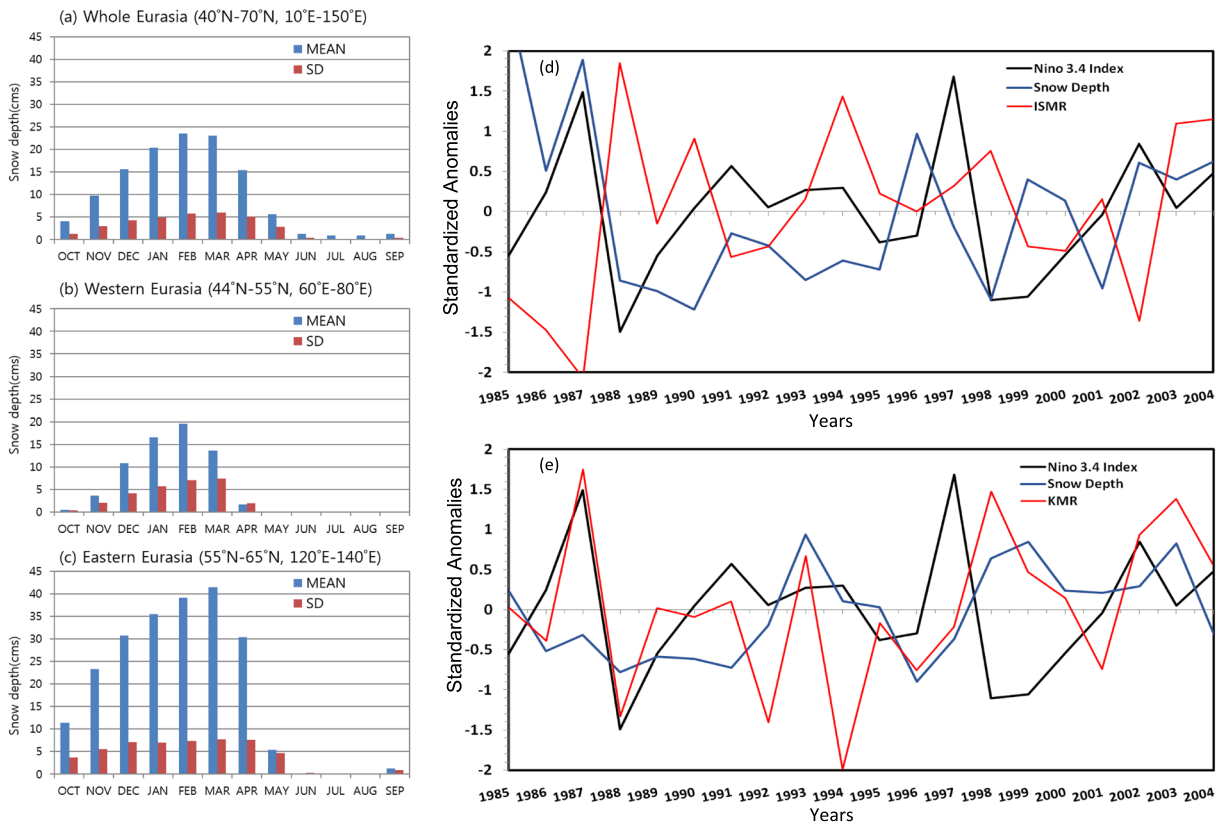


**Figure 2.** Monthly mean values of snow depth (cm) over (a) Whole Eurasia, (b) Western Eurasia, and (c) Eastern Eurasia. Time series of standardized DJF snow depth anomalies during 1985–2004 over (d) western Eurasia (A region of Figure 1a), ISMR anomalies based on IMD data set and Nino 3.4 Index based on JJAS SST anomalies over the region (5°S–5°N, 170°W–120°W), and (e) Eurasia (Q region of Figure 1a), KMR anomalies based on KMA data set and Nino 3.4 Index based on JJAS SST anomalies over the region (5°S–5°N, 170°W–120°W).

relationship of these two regions as identified by Kripalani and Kulkarni (1999); however, here the East Eurasian region is somewhat to the south of the earlier defined position. In the region C (Figure 1a), the CC is positive, but it is not statistically significant.

Figure 1c shows that snow depth anomalies over regions P, Q, and S of Figure 1c in December of the previous year and January and February (DJF) of the current year have positive CCs of about 0.28, 0.46, and 0.31, respectively, with the following KMR. On the other hand, DJF snow depth anomalies over the regions R and T of Figure 1c have negative CCs of about 0.43 and 0.26, respectively, with the subsequent KMR. The CC at regions Q and R is 95% and 90% significant, respectively. This result confirms the relationship of the two regions identified by Kripalani et al. (2002). However, here the regions are not the same as defined by Kripalani et al. (2002) earlier. The other regions of Figure 1c do not yield any statistically significant result.

The snow depth values are used to calculate the standardized snow-depth anomalies by dividing the anomaly of each year from its climatological value by the standard deviation. The standardized snow-depth anomalies calculated over west Eurasia in the region A (Figure 1a) for the period 1985 to 2004 are shown by blue line in Figure 2d. ISMR anomalies are similarly calculated and depicted by the red line. This figure confirms that western Eurasian snow depth is inversely related to ISMR. Earlier, many researchers have shown that there is a negative relationship between the SST anomalies over Nino 3.4 region and ISMR anomalies. This is also evident from Figure 2d. Figure 2e shows that there is a positive relationship between the Eurasian snow depth (box Q) and KMR. Also, the relationship between the Nino-3.4 SST anomalies and KMR is positive as shown in same figure. From the above analysis, it is confirmed that as per ERA Interim snow data set, there is negative relationship between the Western Eurasian snow depth anomalies and ISMR anomalies and positive relationship between Eastern Eurasia snow depth anomalies and KMR anomalies.

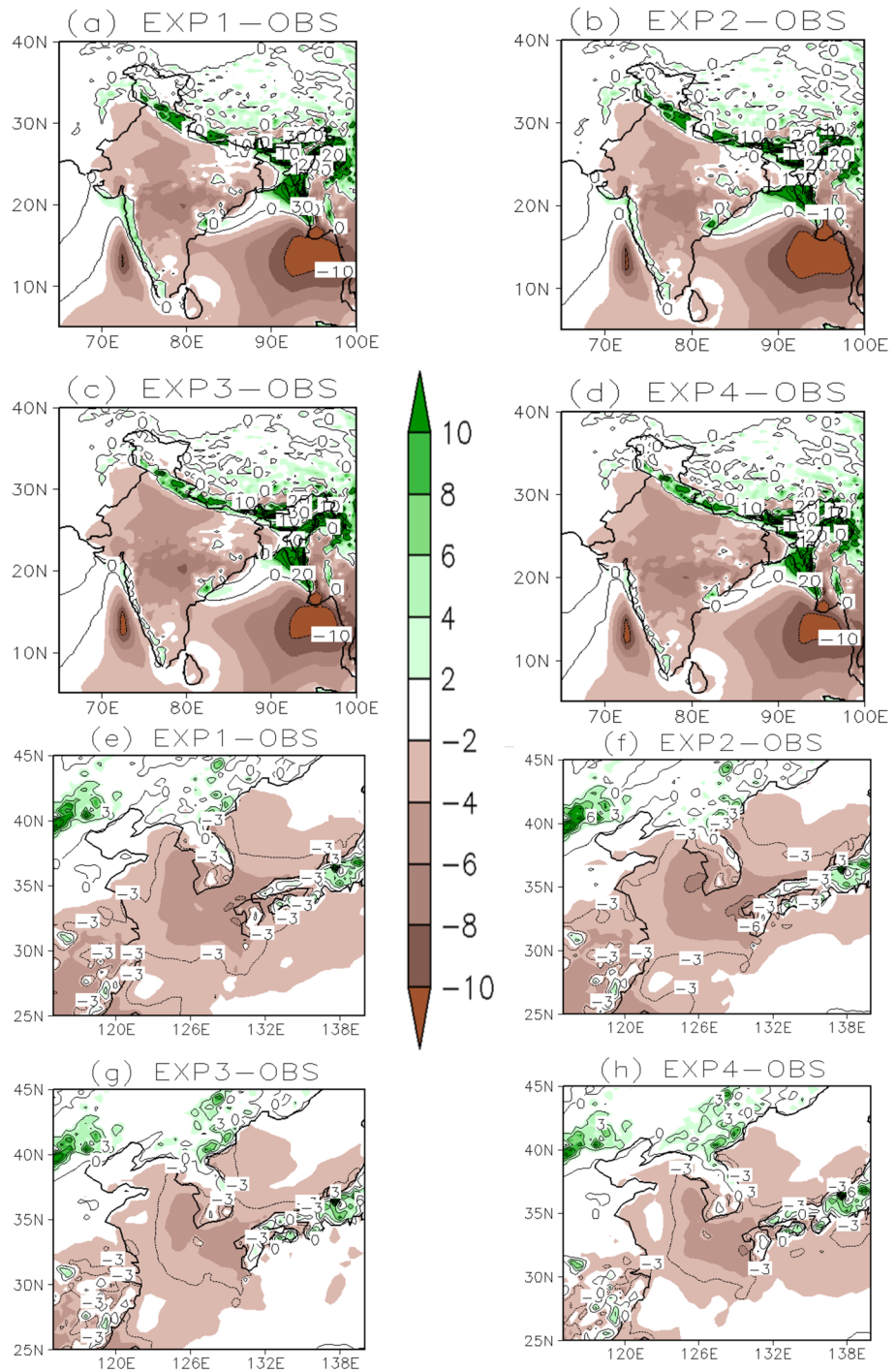


**Figure 3.** Differences of model simulated climatological rainfall (mm/day) and GPCP values in each experiment during the period 1985 to 2004 (a–d) JJAS for India and (e–h) JJA for Korea.

#### 4. Model Bias in all the Experiments

This section compares the model simulated climatological rainfall, winds at 850 and 200 hPa and temperature at 500 hPa for the four experiments with the respective observed fields so as to identify the case with least model bias both over India and Korea. These variables have been illustrated in Figures 3 to 5. The climatological ISMR and KMR for the period 1985 to 2004 have been validated against the corresponding

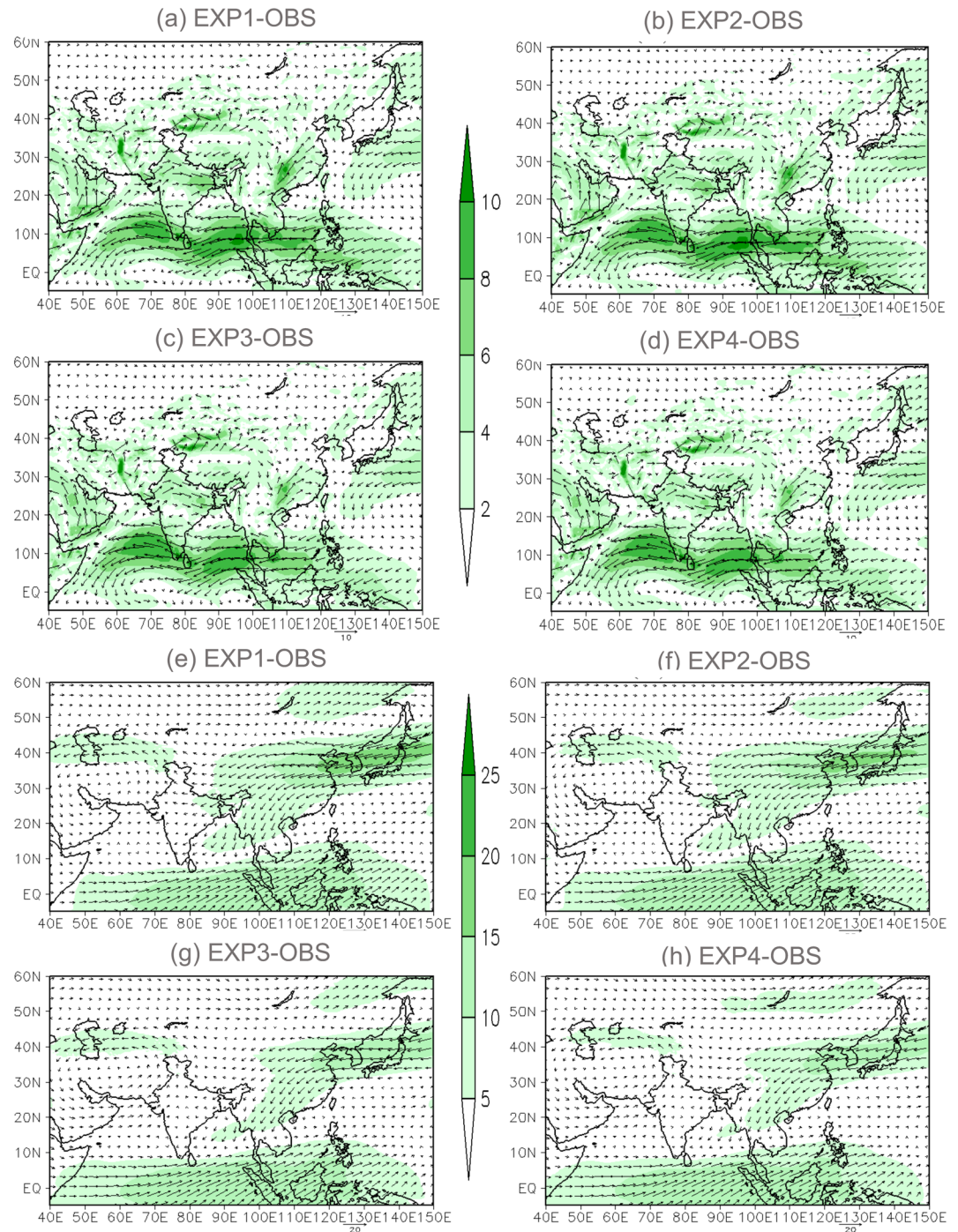


**Figure 4.** Differences of model simulated climatological (a–d) JJAS wind (m/sec) at 850 hPa and (e–h) JJAS wind at 200 hPa and NCEP/NCAR reanalysis in each experiment during the period 1985 to 2004.

observed IMD, GPCP V.2, and KMA data sets. The wind is compared against corresponding NCEP/NCAR reanalyzed data. These results have been discussed in detail in the following subsections.

#### 4.1. Mean Summer Monsoon Rainfall

For the purpose of comparison, the observed GPCP V.2 daily rainfall has been interpolated to 40 km resolution of the model over the Indian and Korean domains. The differences between June, July, August, and



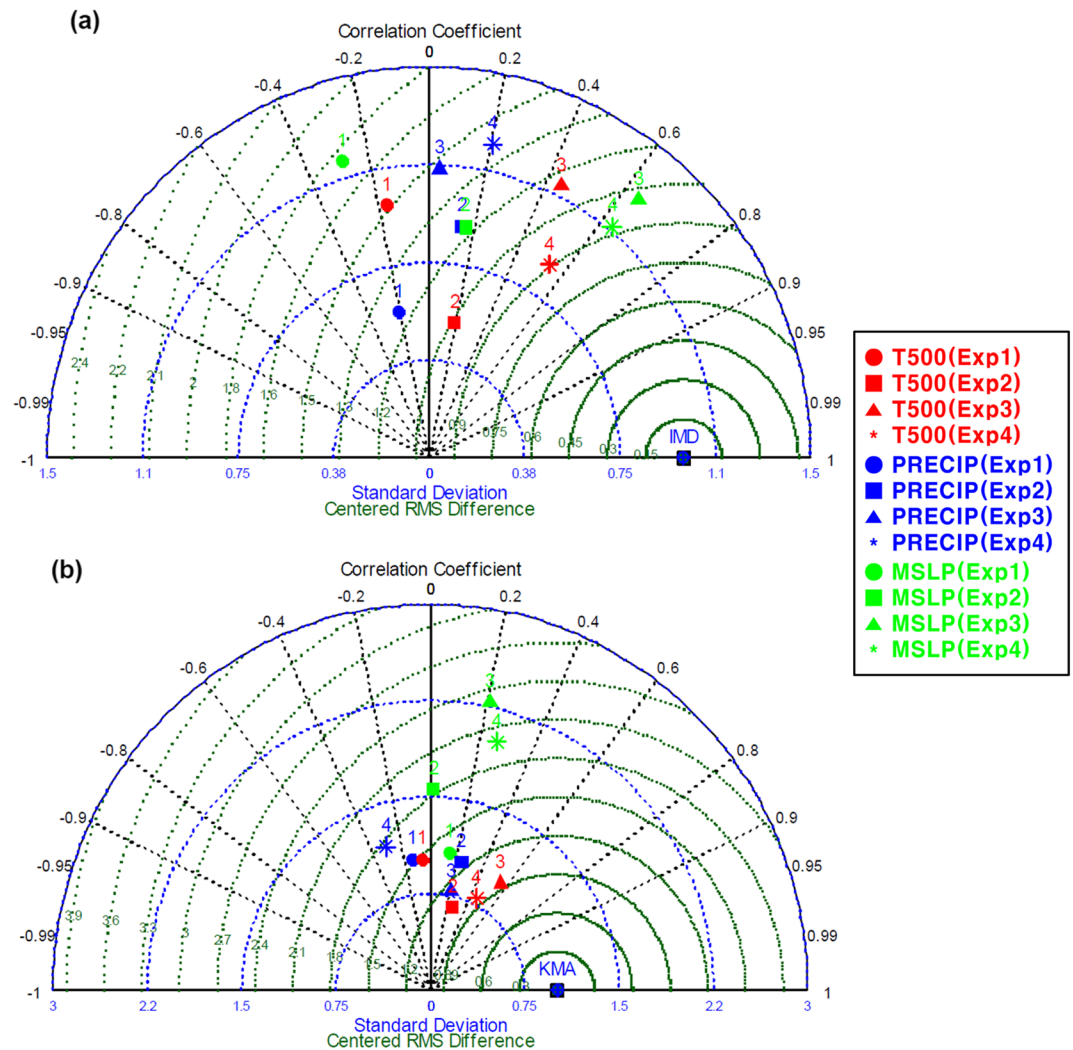


**Figure 5.** Taylor diagram of model simulated climatological variables such as precipitation, temperature at 500 hPa, and mean sea level pressure for the period 1985 to 2004 over (a) India and (b) Korea.

September (JJAS) mean rainfall simulated by GME and obtained from GPCP over India are shown in Figures 3a–3d. JJAS rainfall over India has been underestimated by the model except over west coast, north east, and western Himalaya region. In central India, rainfall is underestimated by about 6 mm/day. In North-East part of India and West Bengal, the rainfall values are overestimated by about 10–30 mm/day in all the experiments. These differences are due to the different boundary conditions as prescribed to the model. In Exp4, the bias is least (6–8 mm/day) in central India compared to rest of the experiments. There is a large extent of negative bias from central India to north west part of India in Exp4. In this experiment, the model has underestimated the rainfall over southern Peninsular and North West India and central India by 6–8 mm/day compared with GPCP rainfall. There is more rainfall bias over the Indian land mass in other experiments. The zonal mean precipitation and time latitude analysis (figure not shown) confirm that the major Indian rainfall belts are well simulated by GME model. The comparison of variability of simulated rainfall and observed GPCP has been examined by the standard deviation of JJAS rainfall in case of India and June, July, and August (JJA) rainfall in case of Korea (figure not shown). The largest amplitude of variability of about 4–5 mm/day is found over the west coast, Bay of Bengal, and north east part of India. The variabilities are more over the regions of large precipitation, and opposite happens in case of less precipitation. GME underestimates the variability compared to observation over the North West part of India in all the experiments.

The differences between JJA simulated rainfall and GPCP rainfall over Korea are shown in Figures 3e–3h. The JJA rainfall simulated by GME is underestimated to a large extent in Exp2 as compared to rest of the experiments. The southern part of Korea has underestimation by about 3 mm/day in Exp1 and Exp3. Less rainfall bias (6–8 mm/day) is seen in Exp4 over Korea land mass. The standard deviation of JJA rainfall (figure not shown) indicates that the amplitude of variability is 2–2.5 mm/day over of the northern part of Korea.

The differences in the spatial patterns of model simulated ISMR and KMR indicate that GME is able to capture both Indian and Korean summer monsoons rainfall well over the large precipitation regions in Exp4 as compared to the rest of the experiments. In general, the GME produces spatial pattern of rainfall and amplitude of the observed variability well in Exp4 in which case both observed SST and snow depth are prescribed as surface boundary conditions to the model.

#### 4.2. Mid-Tropospheric Temperature (500 hPa)

The model simulated temperature at 500 hPa has been compared against that of NCEP/NCAR reanalysis data set. For this purpose, the reanalyzed temperature at 500 hPa has been interpolated to 40 km resolution. Figures S1a–S1d show the differences between JJAS simulated temperature at 500 hPa and NCEP/NCAR reanalysis prevailing over India. In Exp1, the model has simulated warm bias of about 1.5°C over western Himalayas and cold bias by about 1 to 1.5°C over the southern peninsular India. In Exp1 and Exp2, cold bias of about 2.5°C is seen over the Bay of Bengal region. In Exp3 and Exp4, there is no bias over the southern peninsular but warm bias of about 1–2.5°C seen over the North West India. In all the experiments, the model has simulated warm bias over North West and foothills of Himalaya. Least bias is observed over southern peninsula in Exp 4 compared to rest of the experiments. Results show that model simulated temperature at 500 hPa has a good agreement with that of NCEP/NCAR reanalysis in Exp4 among all the four experiments.

The differences between JJA simulated temperature at 500 hPa and NCEP/NCAR reanalysis over the Korea is shown in Figures S1e–S1h. In Exp1 and Exp2, cold bias of about 1.5–2°C is seen over the Oceanic region. The temperature pattern over Korea in Exp3 and Exp4 shows similar spatial pattern as NCEP/NCAR with less bias. There is less bias over the Oceanic regions in Exp 3 and Exp4. Warm bias of low extent is found over Korean land mass in Exp4 as compared against the rest of the three experiments.

#### 4.3. Lower and Upper Wind Circulations

In this subsection, model performance in simulating the monsoon winds at lower (850 hPa) and upper (200 hPa) levels over the Indian and Korean regions is examined. The model simulated winds at 850 and 200 hPa have been compared against the respective NCEP/NCAR reanalysis values. In this study, the reanalyzed wind at both the levels has been interpolated to 40 km of the model resolution.

The comparison between NCEP reanalysis and GME simulated seasonal wind at 850 and 200 hPa are shown in Figures 4a–4d and 4e–4h respectively. The model simulated climatological winds at the two levels in all the experiments are comparable to the respective NCEP/NCAR reanalyzed fields with some differences. The cross equatorial flow, tropical easterly jet, and Tibetan anticyclone represented by the model in Exp4 have some biases as compared to NCEP/NCAR reanalyzed data. The maximum strength of the monsoon flow over the AS is located near 10°–12°N and along 65°–70°E in Exp4. However, core of the Somali jet is shifted to the north in Exp1 and Exp2 in model simulation. The maximum difference of 8 m/sec in the Somali jet over the Arabian Sea in Exp3 and Exp4 is less than that in Exp1 and Exp2. These figures also indicate that the low-level circulation shows weak south westerly flow as compared to the respective observed values. The Somali Jet simulated by the model is weak over western part of Arabian Sea, which remains up to west coast of India and some parts of peninsular India in Exp4 compared to rest of the experiments.

The climatological difference of model simulated upper level wind from NCEP/NCAR in each of the experiments is shown in Figures 4e–4h. The location of the Tibetan anticyclone over the South Asian region agrees well with NCEP/NCAR reanalysis in Exp4 as compared to rest of the experiments, and hence, Figure 4h shows least wind bias. Difference of about 5–10 m/sec is observed over Tibet in Exp1, and it diminishes in Exp2 and becomes the least in Exp4. The difference of Tropical Easter Jet (TEJ) over the Bay of Bengal is about 5–10 m/sec in Exp1 and Exp3. The strength of the TEJ is well simulated in Exp2 and Exp4 as when the observed snow is prescribed to the model as boundary conditions.

The maximum strengths of monsoon wind at upper and lower levels over the Indian and Korean regions have been calculated and compared against the respective NCEP/NCAR reanalyzed values. The maximum wind strengths at 850 hPa along the Arabian Sea region (8°N–12°N, 50°E–60°E) in Exp4 and Exp2 are 17.6 and 17.6 m/sec, respectively, against 16.4 m/sec in NCEP/NCAR reanalysis. In case of Korean region (34°N–40°N, 125°E–130°E) the maximum wind strengths are 6.7 and 7.2 m/sec in Exp4 and Exp2, respectively, against 5.4 m/sec in NCEP/NCAR. Thus, one can infer that the wind and the maximum strength in the lower troposphere are well simulated in Exp4 and Exp2. The maximum wind strength of TEJ in the region bounded by 5°N–20°N and 70°E–90°E in Exp4 and Exp2 are 22.1 and 23.9 m/sec, respectively, against 23.5 m/sec in NCEP/NCAR reanalysis. The maximum TEJ strengths over the Korean region (34°N–40°N, 125°E–130°E) are 17.5 and 16.3 m/sec in Exp4 and Exp2, respectively, against 26.6 m/sec in NCEP/NCAR reanalysis.

From the above analysis, it is seen that the model climatology of winds in the lower and upper levels simulated in Exp4 is similar to the observed climatology represented by NCEP/NCAR data. The position of the model simulated low level jet is slightly shifted to the north as compared with that of NCEP/NCAR reanalysis. The wind strength at both the levels in Exp4 and Exp2 are very close to the respective reanalyzed values. The wind patterns at lower and upper levels are well simulated in Exp4 and Exp2 when observed snow is prescribed into the model. This fact highlights the relative role of observed snow as against the observed SST as surface boundary condition to the model.

## 5. Model Performance using Taylor Diagram

In order to get a more quantitative picture of how well (or how poorly) the model experiments agree with observations, a Taylor diagram (Taylor, 2001) has been prepared and shown in Figure 5. This diagram enables visualization of three quantities standard deviation normalized by observation, correlation with observation, and Root Mean Square Error (RMSE) in a two-dimensional space. This is possible because the three quantities are not independent of each other. The polar coordinate of the diagram gives the correlation between model and observation for space-time variations but contains no information about the amplitude of the variations. The IMD JJAS and KMA JJA rainfall, temperature at 500 hPa, and Mean Sea Level Pressure (MSLP) data sets have been interpolated to a common grid resolution of 40 km during the period 1985–2004 for the comparison. Figures 5a and 5b represent the Taylor diagram of model simulated climatological variables such as precipitation, temperature at 500 hPa, and MSLP for the period 1985 to 2004 over the India and Korea region, respectively. The simulated SD values of ISMR are 0.7, 0.8, 1.0, and 0.8 mm/day in Exp1, Exp2, Exp3, and Exp4, respectively, against the observed values of 0.5 mm/day. The simulated SD values of KMR are 1.8, 1.8, 1.4, and 2.1 mm/day in Exp1, Exp2, Exp3, and Exp4, respectively, against the observed values of 1.8 mm/day. RMSE calculated from GME for ISMR precipitation in Exp1, Exp2, Exp3, and Exp4 is 0.75, 1.0, 0.90, and 1.0 mm/day, respectively. It is seen that the RMSE is slightly more in Exp2 and Exp4 than Exp1 and Exp3. The CC between the GME simulated and IMD rainfall during JJAS are –2.0, 0.14, 0.03, and 0.20 in Exp1, Exp2, Exp3, and Exp4, respectively. The ISMR and KMR have been relatively poorly correlated with respective IMD and KMA observed values, respectively. The CC between the temperature at 500 hPa and NCEP/NCAR reanalysis in India and Korea regions describes that Exp4 and Exp3 are better than those of Exp2 and Exp1. Another important variable such as MSLP is used for model performance evaluation in terms of monsoon processes over India and Korea. The CC between model simulated MSLP over India is found to be 0.6 in Exp4 and Exp3, respectively. From the above analysis, it is seen that observed snow and SST prescribed into the model (as in Exp4) yield the best values of all the important monsoon parameters.

## 6. Intercomparison of Model Sensitivity Experiments

As described earlier, the GME has been prescribed with observed SST in Exp3 and Exp4 and observed snow in Exp2 and Exp4. The differences of Exp4-Exp1, Exp4-Exp2, and Exp4-Exp3 in case of rainfall, temperature at 500 hPa, and wind at both the levels are analyzed in this subsection in details. The difference between Exp4 and Exp1 indicates the combined role of observed SST and snow in comparison to that of climatological SST and snow. The difference between Exp4 and Exp3 is the measure of observed snow alone in comparison to its climatological values in the presence of observed SSTs. Similarly, the role of observed SST alone as

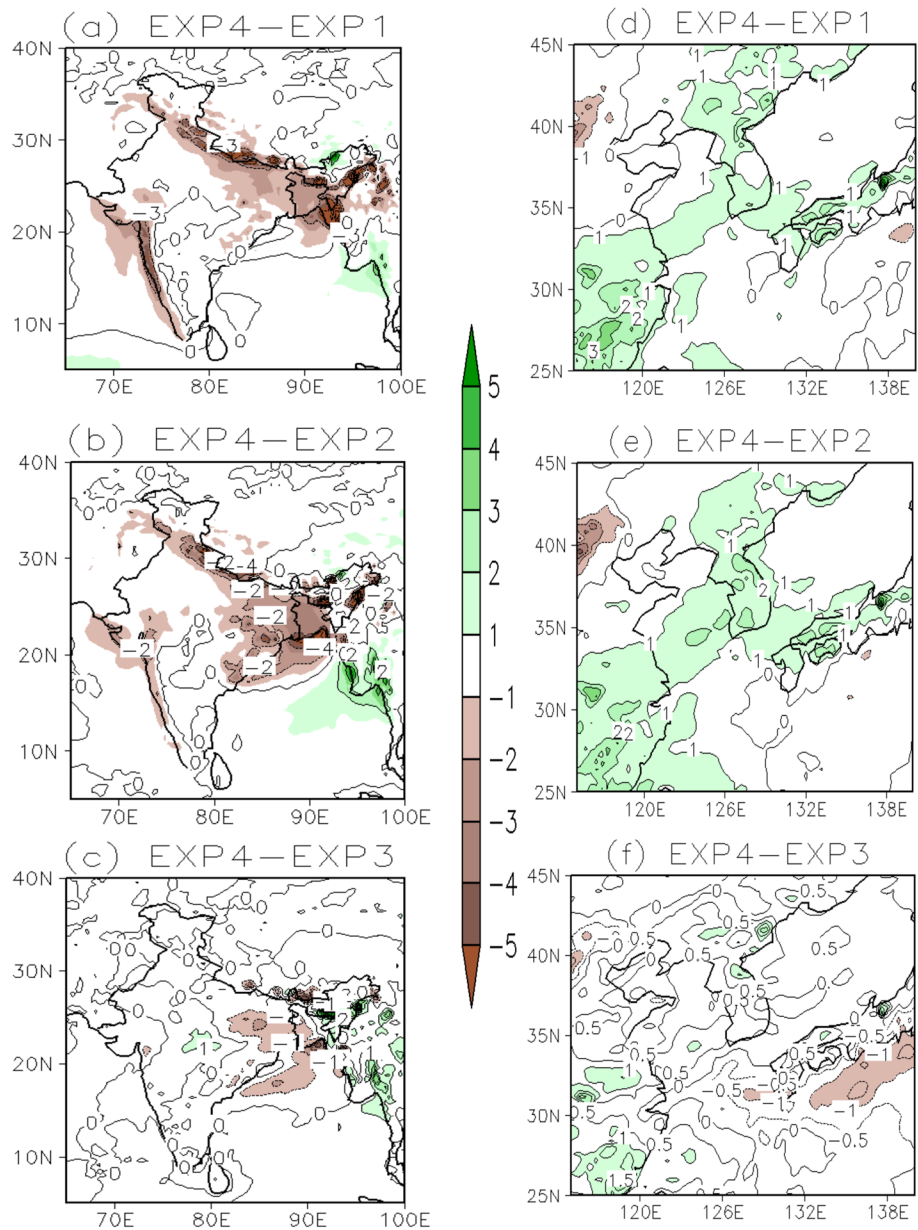


**Figure 6.** Differences of model simulated climatological rainfall (mm/day) between the experiments during the period 1985 to 2004, (a–c) JJAS for India and (d–f) JJA for Korea.

against climatological SST in the presence of observed snow has been indicated in the difference between the Exp4 and Exp2.

Here, the difference of model simulated climatology of ISMR and KMR among the four experiments for the period 1984 to 2005 are analyzed. The differences of model simulated climatological rainfall (mm/day) between the sensitivity experiments have been shown in Figures 6a–6c (JJAS for India) and Figures 6d–6f (JJA for Korea region). Figure 6a explains that JJAS rainfall is overestimated by about 1–3 mm/day over east coast of India, north east India, and foothills of Himalaya in Exp1. Since Exp3 has been prescribed by observed SST as boundary condition, the model is underestimated by 1 mm/day in Exp4 over east coast of India (Figure 6c). The rainfall difference is less between Exp4 and Exp3 over the central part of India compared to rest of the experiments. However, the rainfall difference is less over the Western Ghats, which may be attributed to the model's coarser resolution in resolving the hilly region as compared to rest of the

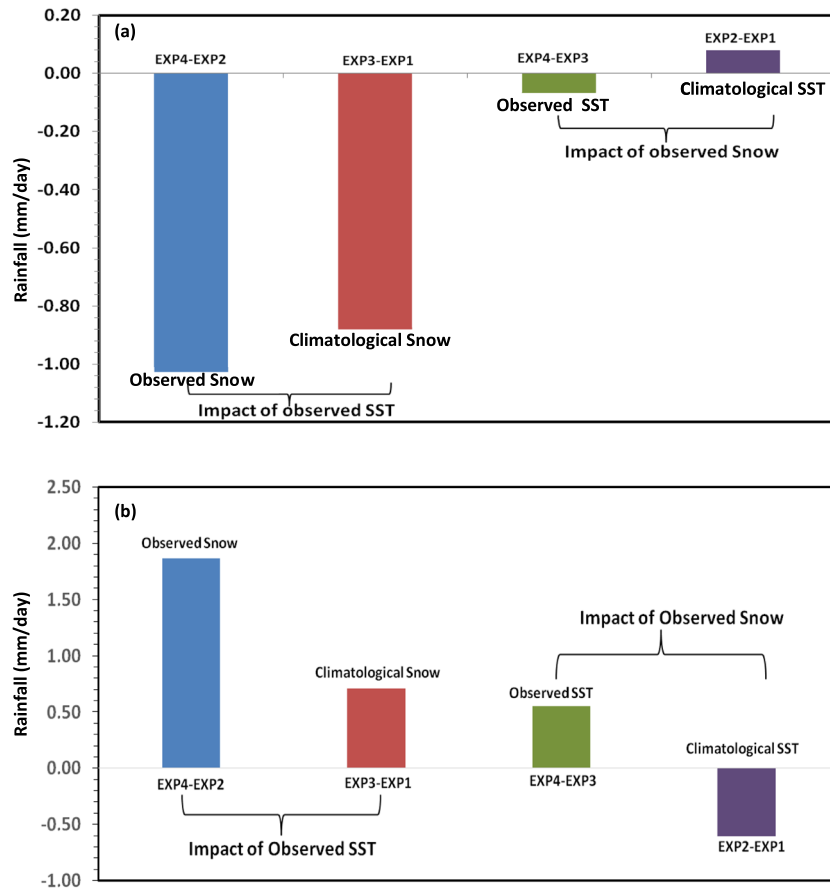


**Figure 7.** Differences in (a) JJAS mean rainfall climatologies for India and (b) JJA mean rainfall climatologies for Korea among the four sensitivity experiments.

experiments. Figure 6b shows that Exp2 (observed snow and climatological SST prescribed into the model) has overestimated JJAS rainfall by about 2 mm/day rainfall over the east coast and north east of India as compared to Exp4. There is an overestimation of rainfall of about 2 mm/day over the Korean region in Exp4 compared to Exp2 (Figure 6e). It is worthy to point out that the largest rainfall differences are confined only to certain regions, which is so-called rainfall-sensitive region. There is no rainfall difference over Korea (Figure 6f) due to the observed SST prescribed into the GME. From the above analysis, it is revealed that the model well simulates summer monsoon rainfall over the Indian and Korean regions with the prescribed observed SST. However, with the inclusion of observed snow along with observed SST into the GME, the monsoon rainfall values are closer to their observed values.

The impact of SST and snow on ISMR and KMR is shown in Figures 7a and 7b respectively. The relative impact of observed and climatological snow can be accessed from the differences Exp4-Exp3 and Exp2-Exp1, respectively. Similarly, the effect of observed and climatology SST can be accessed from the difference of Exp4-Exp2 and Exp3-Exp1, respectively. These figures (Exp4-Exp3, Exp2-Exp1, Exp4-Exp2, and Exp3-Exp1) are obtained from the differences in JJAS/JJA mean rainfall climatologies for India/Korea, respectively, during the period 1985 to 2004. Figure 7a shows the negative impacts of both the climatology and observed SST. Further, the SST impact dominates over that of snow to the extent that snow impact on ISMR is 1.1% of the SST impact. Although the impact of snow is less, when the observed snow is added to observed SST then simulated ISMR gets better. The percentages of impact Exp4-Exp2, Exp3-Exp1, Exp4-Exp3, and Exp2-Exp1 with respect to Exp4-Exp1 are 108%, 92%, 7%, and -8%, respectively, over India. The differences Exp4-Exp3 and Exp2-Exp1 over the Korean region (Figure 7b) describe that the influence of snow and SST is just opposite to that in India. Figure 7b depicts the impacts of both the climatology and observed SST on the positive side. The percentages of impact Exp4-Exp2, Exp3-Exp1, Exp4-Exp3,

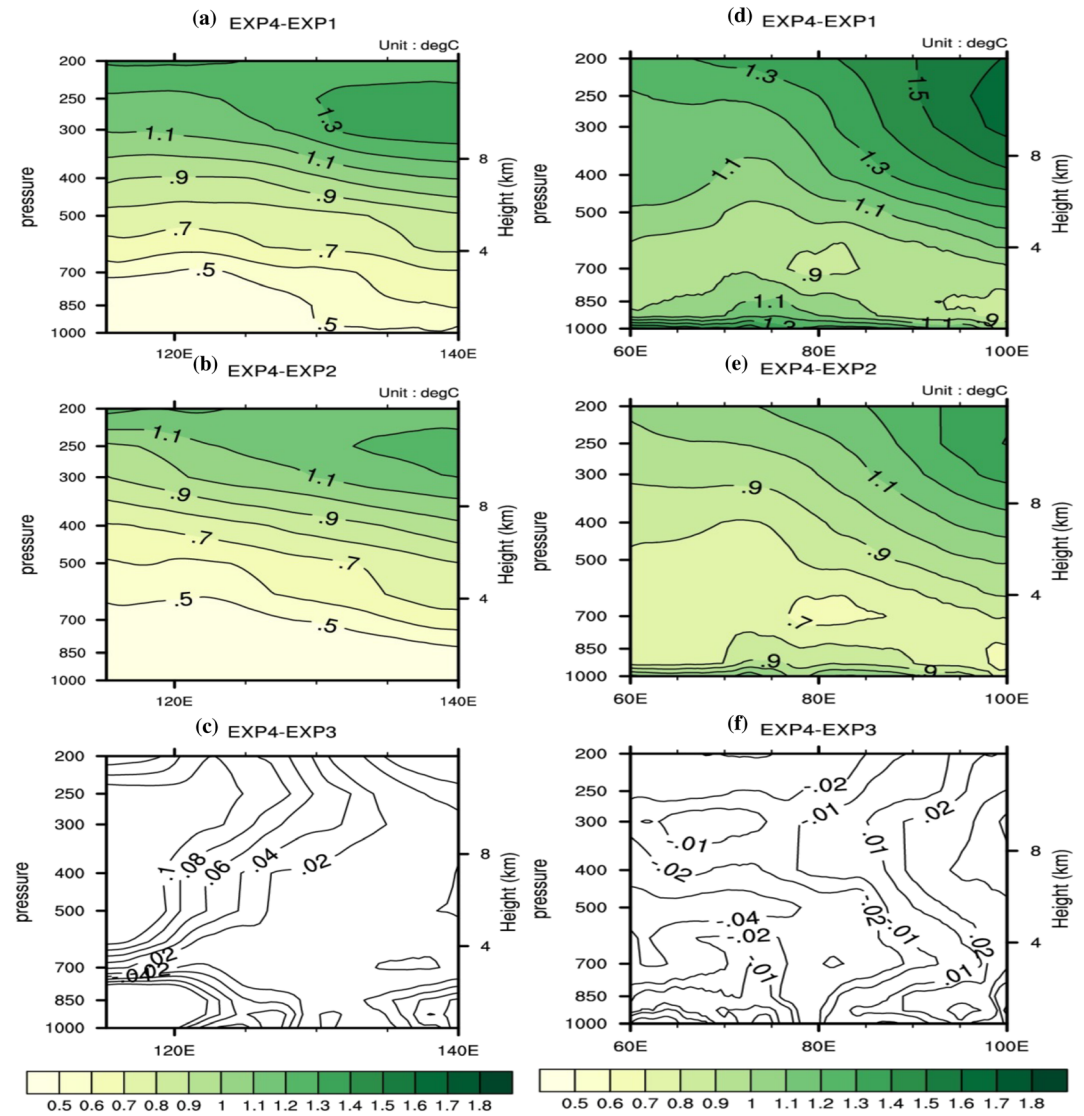


**Figure 8.** Differences of longitude pressure cross sections of the GME simulated JJAS mean air temperatures between the experiments. Left panel is meridionally averaged over 5°S to 40°N, and right panel is meridionally averaged over 25°N to 45°N.

and Exp2-Exp1 with respect to Exp4-Exp1 are 147%, 56%, 44%, and -48%, respectively, over Korea. The above analysis reveals that the impact of SST plays a dominant role over the Indian and Korean monsoons. Without the inclusion of observed snow as boundary conditions to the GME, simulated ISMR and KMR are not close to observed values. The inclusion of observed snow with observed SST as boundary condition improves the model simulation of ISMR and KMR.

The differences of model simulated climatological temperature at 500 hPa among the four experiments are shown in Figures S2a–S2c (JJAS for India) and Figures S2d–S2f (JJA for Korea). In Figure S2a, the temperature difference of about 1.2°C is found over southern and north east part of India. The model simulated temperature over Indian land using observed snow depth and SST is more than obtained from the experiment with climatological snow and SST. Figure S2b shows that temperature differences of about 0.2°C to 0.9°C and 1.1°C are seen over northern and southern parts of India, respectively. Figures S2d and S2e depict the spatial pattern of temperature differences of about 0.6°C to 0.9°C over Korea. Least difference in temperature is seen in Figures S2c and S2f over Indian and Korean land, where observed SST is prescribed to the GME. However, comparison of Figure S2a with Figure S2b and Figure S2d with Figure S2e indicates that observed

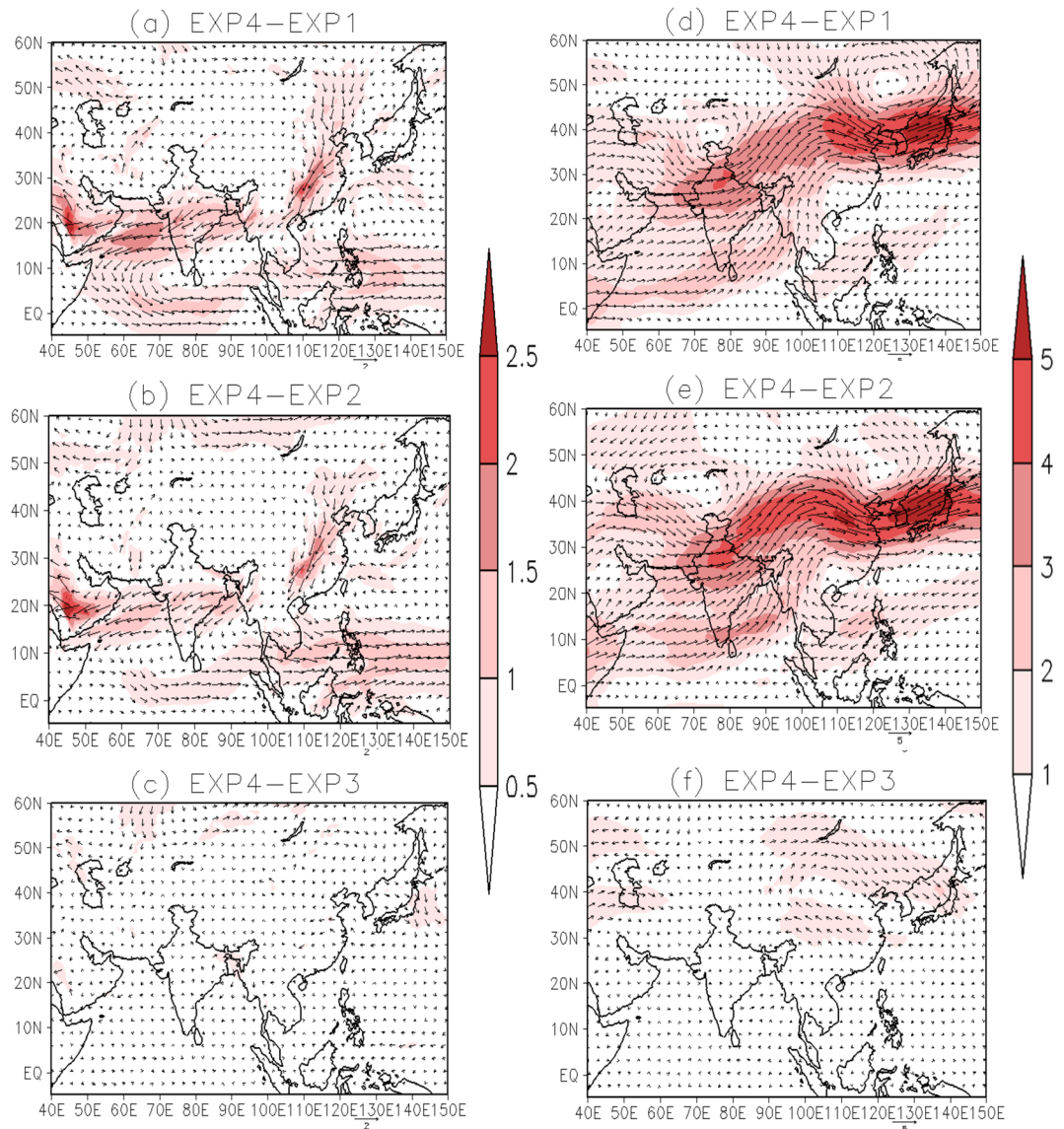


**Figure 9.** Differences of model simulated climatological (a–c) JJAS wind (m/sec) at 850 hPa and (d–f) JJAS wind at 200 hPa between the experiments during the period 1985 to 2004.

snow also plays an important role in simulating the monsoon temperature at Indian and Korean regions in comparison to boundary conditions such as climatological snow and SST prescribed to GME.

The longitudinal-pressure cross sections of the model simulated JJAS mean air temperature differences between the experiments are depicted in Figure 8. Left panel of the figure depicts JJAS temperature meridionally averaged from 5°S to 40°N. The difference Exp4-Exp2 is closer to the surface and large in the upper troposphere, which is the impact of observed snow compared to climatological snow in the presence of observed SST. In contrast, there is less impact of observed SST against climatological SST in the presence of observed snow (Exp4-Exp3). The longitudinal-pressure cross sections of JJA temperature differences between the experiments are depicted in right side panel of figure. The JJA temperature (Figures 8d–8f) is meridionally averaged 25°N to 45°N. Similar results as in case of India are noticed. Figures 8c and 8f indicate that JJAS temperature difference over India and JJA temperature difference over Korea are the least in case of Exp4-Exp3, which highlights the role of observed snow as against climatological snow in the presence of observed SST.

The differences of model simulated climatological JJAS winds (m/sec) between the sensitivity experiments are shown in Figures 9a–9c (850 hPa) and Figures 9d–9f (200 hPa) during the period 1985 to 2004. Figures 9a

and 9b depict difference of winds at 850 hPa between Exp4 and Exp1 and Exp4 and Exp2 simulated in GME, respectively. Figure 9a shows that the low-level jet simulated by the model in Exp4 is weaker in its wind strength by 1.5–2 m/s than Exp1 and 1–1.5 m/s than Exp2 over the north of Arabian sea. It is seen that the westerly wind is weaker in Exp1 compared to Exp2 and least in Exp3. Therefore, the magnitude of westerly wind over the central India stronger by about 2 m/sec in Exp2 as compared to Exp1. The strength of winds in Exp2 over the Bay of Bengal is stronger by about 1–2 m/sec as compared to Exp1. Figure 9c shows that there is less difference in wind between the Exp4 and Exp3 at lower level over India and Korea. The observed SST plays a dominant role in representing the wind realistically at 850 hPa. The differences of wind strength are less at lower level when the observed snow has been replaced by observed SST.

It has been explained in the earlier section that the observed values of SST and snow (i.e., Exp4) produce the upper level easterlies realistically in the model. So, the differences of upper level (200 hPa) winds between the sensitivity experiments are depicted in Figures 9d–9f. Figure 9d shows that the upper level easterly wind simulated by the model in Exp4 is weaker compared to Exp1. It is seen that the TEJ is weaker in Exp1 compared to Exp2 and least in Exp3. Therefore, TEJ in Exp2 is stronger by about 2 m/sec as compared to Exp1. The wind strength is improved by 1 m/sec over the southern peninsula and Bay of Bengal when the observed snow (i.e., Exp2) is replaced by climatological snow and SST (i.e., Exp1) into the model. The Tibetan anticyclone is improved in Exp2 compared to Exp1. The representation of interannual variation in observed snow is more accurate than the climatological snow. Figure 9f shows that there is less difference in wind between the Exp4 and Exp3 at upper level over the India and Korea region. The observed SST plays a dominant role in representing the wind realistically at 200 hPa. The strength of the easterly wind has stronger by about 2 m/sec in Exp2 compared to Exp1 over the Korea region. The inclusion of observed SST into the model GME improves the circulation pattern over both the regions.

## 7. Discussion and Conclusions

In this study, the relative roles of the two most important boundary conditions such as SST and Eurasian snow on the Indian and Korean monsoons have been examined using the high resolution (40 km) global numerical weather prediction model of German Weather Service (Deutscher Wetterdienst) called GME. The GME has been integrated at PKNU, Busan, South Korea from 25 April to 30 September in each of the years covering the period 1985 to 2004. Four sensitivity experiments have been conducted by using climatological as well as observed values of snow and SST. In Exp1 climatological SST and Snow depth are used, Exp2 uses the climatological SST and observed Snow depth, Exp3 has observed SST and climatological Snow depth, and finally in Exp4 observed SST and Snow depth are provided as boundary conditions. Results show that the model simulates the spatial distributions of Indian and Korean summer monsoon rainfall in all the experiments, with varying biases. GME simulated Indian and Korean monsoon rainfall in Exp4 has the least bias with respect to observed rainfall values of GPCP in comparison to other three experiments. GME also produced the spatial pattern and amplitude of the observed variability reasonably well in Exp4. The wind speeds (m/sec) at 850 and 200 hPa have also been computed for the Indian and Korean Monsoons. The cross equatorial flow, tropical easterly jet, and Tibetan anticyclone represented by the model in experiments have some biases as compared to NCEP/NCAR reanalyzed data. The maximum strength of the monsoon flow over the AS is located near 10°–12°N and along 65°–70°E in Exp4. However, core of the Somali jet is shifted to the north in Exp1 and Exp2 in model simulation.

The relative roles of observed and climatological snow have been examined from the difference fields Exp4-Exp3 and Exp2-Exp1 in case of the variables such as precipitation, winds at 850 and 200 hPa, and temperature at 500 hPa, respectively. Similarly, the roles of observed and climatology SST have been analyzed from the difference of Exp4-Exp2 and Exp3-Exp1. Comparison of simulated ISMR and KMR differences such as Exp4-Exp1, Exp4-Exp2, and Exp4-Exp3 shows that GME is able to capture both Indian and Korean monsoon rain well with the prescribed observed SST (Exp4-Exp2) in the presence of observed snow. Thus, the effect of observed snow (Exp4-Exp2) in addition to observed SST in the model is important to simulate both the monsoons well. In sum, the results of this study point to the fact that the model simulated summer monsoon circulation and rainfall in India and Korea are not adequately simulated unless observed Eurasian snow depth is prescribed to GME in addition to the observed SST.



## Data Availability Statement

All data used in this study are freely available and can be requested from the authors or obtained directly from the source: GPCP V.2 daily rainfall (<https://climatedataguide.ucar.edu/climate-data/gpcp-monthly-global-precipitation-climatology-project>), ERA-Interim (<https://www.ecmwf.int/en/forecasts/datasets/reanalysis-datasets/era-interim>), SST (<https://www.ncdc.noaa.gov/oisst>), GME ([www.dwd.de](http://www.dwd.de) > downloads > nwp > gme > gme\_users\_guide\_2\_32\_en), and wind and temperature of NCEP/NCAR reanalysis (<https://www.esrl.noaa.gov/psd/data/gridded/data.ncep.reanalysis.html>), and IMD has been obtained from India Meteorology Department Pune India.

## Conflict of Interest

The authors declare no competing interests.

## Acknowledgments

This work was jointly supported by the Department of Science and Technology (DST), Government of India, (DST No: INT/Korea/P-06/2011) and the Korea Meteorological Administration Research and Development Program under Grant CATER 2012-7150. The authors would like to acknowledge the support from KISTI supercomputing center through the strategic support program for the supercomputing application research (No. KSC-2012-C2-64). KCP acknowledges the support from the NERC (UK Natural Environment Research Council) AMAZONICA and Amazon Hydrological Cycle grants (NE/F005806/1 and NE/K01353X/1). We acknowledge GME, ECMWF, IMD, GPCP, KMA, and NCEP/NCAR for providing data.

## References

- Adler, R. F., Huffman, G. J., Chang, A., Ferraro, R., Xie, P.-P., Janowiak, J., et al. (2003). The Version-2 global precipitation climatology project (GPCP) monthly precipitation analysis (1979–present). *Journal of Hydrometeorology*, 4(6), 1147–1167. [https://doi.org/10.1175/1525-7541\(2003\)004<1147:Tvgpcp>2.0.Co;2](https://doi.org/10.1175/1525-7541(2003)004<1147:Tvgpcp>2.0.Co;2)
- Bamzai, A. S., & Shukla, J. (1999). Relation between Eurasian snow cover, snow depth, and the Indian summer monsoon: An observational study. *Journal of Climate*, 12(10), 3117–3132. [https://doi.org/10.1175/1520-0442\(1999\)012<3117:Rbescs>2.0.Co;2](https://doi.org/10.1175/1520-0442(1999)012<3117:Rbescs>2.0.Co;2)
- Barnett, T. P., Dümenil, L., Schlese, U., Roeckner, E., & Latif, M. (1989). The effect of Eurasian snow cover on regional and global climate variations. *Journal of the Atmospheric Sciences*, 46(5), 661–686. [https://doi.org/10.1175/1520-0469\(1989\)046<0661:Teosc>2.0.Co;2](https://doi.org/10.1175/1520-0469(1989)046<0661:Teosc>2.0.Co;2)
- Blanford, H. F. (1884). On the connexion of the Himalaya snowfall with dry winds and seasons of drought in India. *Proceedings of the Royal Society of London*, 37(232-234), 3–22. <https://doi.org/10.1098/rspl.1884.0003>
- Cess, R. D., Potter, G. L., Zhang, M.-H., Blanchet, J.-P., Chalita, S., Colman, R., et al. (1991). Interpretation of snow-climate feedback as reproduced by 17 general circulation models. *Science*, 253(5022), 888–892. <https://doi.org/10.1126/science.253.5022.888>
- Charney, J. G., & Shukla, J. (1981). In J. Lighthill & R. P. Pearce (Eds.), *Predictability of monsoons. Monsoon Dynamics* (pp. 99–109). UK: Cambridge University Press.
- Cohen, J., & Rind, D. (1991). The effect of snow cover on the climate. *Journal of Climate*, 4(7), 689–706. [https://doi.org/10.1175/1520-0442\(1991\)004<0689:teosco>2.0.co;2](https://doi.org/10.1175/1520-0442(1991)004<0689:teosco>2.0.co;2)
- Dash, S. K., Kulkarni, M. A., Mohanty, U. C., & Prasad, K. (2009). Changes in the characteristics of rain events in India. *Journal of Geophysical Research*, 114, D10109. <https://doi.org/10.1029/2008jd010572>
- Dash, S. K., Parth Sarthi, P., & Panda, S. K. (2006). A study on the effect of Eurasian snow on the summer monsoon circulation and rainfall using a spectral GCM. *International Journal of Climatology*, 26(8), 1017–1025. <https://doi.org/10.1002/joc.1299>
- Dash, S. K., Singh, G. P., Shekhar, M. S., & Vernekar, A. D. (2004). Response of the Indian summer monsoon circulation and rainfall to seasonal snow depth anomaly over Eurasia. *Climate Dynamics*, 24(1), 1–10. <https://doi.org/10.1007/s00382-004-0448-3>
- Dee, D. P., Uppala, S. M., Simmons, A. J., Berrisford, P., Poli, P., Kobayashi, S., et al. (2011). The ERA-interim reanalysis: Configuration and performance of the data assimilation system. *Quarterly Journal of the Royal Meteorological Society*, 137(656), 553–597. <https://doi.org/10.1002/qj.828>
- Douville, H., & Royer, J. F. (1996). Sensitivity of the Asian summer monsoon to an anomalous Eurasian snow cover within the Météo-France GCM. *Climate Dynamics*, 12(7), 449–466. <https://doi.org/10.1007/bf02346818>
- Fasullo, J. (2004). A stratified diagnosis of the Indian monsoon—Eurasian snow cover relationship. *Journal of Climate*, 17(5), 1110–1122. [https://doi.org/10.1175/1520-0442\(2004\)017<1110:Asdoti>2.0.Co;2](https://doi.org/10.1175/1520-0442(2004)017<1110:Asdoti>2.0.Co;2)
- Ferranti, L., & Molteni, F. (1999). Ensemble simulations of eurasian snow-depth anomalies and their influence on the summer Asian monsoon. *Quarterly Journal of the Royal Meteorological Society*, 125(559), 2597–2610. <https://doi.org/10.1002/qj.4971255913>
- Goswami, B. N., Venugopal, V., Sengupta, D., Madhusoodanan, M. S., & Xavier, P. K. (2006). Increasing trend of extreme rain events over India in a warming environment. *Science*, 314(5804), 1442–1445. <https://doi.org/10.1126/science.1132027>
- Kalnay, E., Kanamitsu, M., Kistler, R., Collins, W., Deaven, D., Gandin, L., et al. (1996). The NCEP/NCAR 40-year reanalysis project. *Bulletin of the American Meteorological Society*, 77(3), 437–471. [https://doi.org/10.1175/1520-0477\(1996\)077<0437:Tnyrp>2.0.Co;2](https://doi.org/10.1175/1520-0477(1996)077<0437:Tnyrp>2.0.Co;2)
- Karri, S., Dash, S. K., Panda, S. K., Paliwal, M., Mishra, S. K., & Oh, J.-H. (2018). Relative role of sea surface temperature and snow on Indian summer monsoon seasonal simulation using a GCM. *Arabian Journal of Geosciences*, 11(9), 210. <https://doi.org/10.1007/s12517-018-3559-6>
- Keshavamurty, R. N. (1982). Response of the atmosphere to sea surface temperature anomalies over the equatorial Pacific and the teleconnections of the southern oscillation. *Journal of the Atmospheric Sciences*, 39(6), 1241–1259. [https://doi.org/10.1175/1520-0469\(1982\)039<1241:Rotats>2.0.Co;2](https://doi.org/10.1175/1520-0469(1982)039<1241:Rotats>2.0.Co;2)
- Kirtman, B. P., & Shukla, J. (2000). Influence of the Indian summer monsoon on ENSO. *Quarterly Journal of the Royal Meteorological Society*, 126(562), 213–239. <https://doi.org/10.1002/qj.49712656211>
- Kripalani, R. H., Kim, B.-J., Oh, J.-H., & Moon, S.-E. (2002). Relationship between soviet snow and Korean rainfall. *International Journal of Climatology*, 22(11), 1313–1325. <https://doi.org/10.1002/joc.809>
- Kripalani, R. H., & Kulkarni, A. (1999). Climatology and variability of historical soviet snow depth data: Some new perspectives in snow - Indian monsoon teleconnections. *Climate Dynamics*, 15(6), 475–489. <https://doi.org/10.1007/s003820050294>
- Liu, X., & Yanai, M. (2002). Influence of Eurasian spring snow cover on Asian summer rainfall. *International Journal of Climatology*, 22(9), 1075–1089. <https://doi.org/10.1002/joc.784>
- Majewski, D., Liermann, D., Prohl, P., Ritter, B., Buchhold, M., Hanisch, T., et al. (2002). The operational global icosahedral-hexagonal Gridpoint model GME: Description and high-resolution tests. *Monthly Weather Review*, 130(2), 319–338. [https://doi.org/10.1175/1520-0493\(2002\)130<0319:Togihg>2.0.Co;2](https://doi.org/10.1175/1520-0493(2002)130<0319:Togihg>2.0.Co;2)
- Meehl, G. A., & Washington, W. M. (1990). CO<sub>2</sub> climate sensitivity and snow-sea-ice albedo parameterization in an atmospheric GCM coupled to a mixed-layer ocean model. *Climatic Change*, 16(3), 283–306. <https://doi.org/10.1007/bf00144505>

- Mooley, D. A., & Parthasarathy, B. (1984). Fluctuations in all-India summer monsoon rainfall during 1871–1978. *Climatic Change*, *6*(3), 287–301. <https://doi.org/10.1007/bf00142477>
- Morinaga, Y., Tian, S.-F., & Shinoda, M. (2003). Winter snow anomaly and atmospheric circulation in Mongolia. *International Journal of Climatology*, *23*(13), 1627–1636. <https://doi.org/10.1002/joc.961>
- Oh, J.-H., Kwon, W.-T., & Ryoo, S.-B. (1997). Review of the researches on changma and future observational study (kormex). *Advances in Atmospheric Sciences*, *14*(2), 207–222. <https://doi.org/10.1007/s00376-997-0020-2>
- Ose, T. (1996). The comparison of the simulated response to the regional snow mass anomalies over Tibet, Eastern Europe, and Siberia. *Journal of the Meteorological Society of Japan. Ser. II*, *74*(6), 845–866. [https://doi.org/10.2151/jmsj1965.74.6\\_845](https://doi.org/10.2151/jmsj1965.74.6_845)
- Palmer, T. N., Branković, Č., Viterbo, P., & Miller, M. J. (1992). Modeling interannual variations of summer monsoons. *Journal of Climate*, *5*(5), 399–417. [https://doi.org/10.1175/1520-0442\(1992\)005<0399:Mivosm>2.0.Co;2](https://doi.org/10.1175/1520-0442(1992)005<0399:Mivosm>2.0.Co;2)
- Panda, S. K., Dash, S. K., Bhaskaran, B., & Pattnayak, K. C. (2016). Investigation of the snow-monsoon relationship in a warming atmosphere using Hadley Centre climate model. *Global and Planetary Change*, *147*, 125–136. <https://doi.org/10.1016/j.gloplacha.2016.10.013>
- Parthasarathy, B., & Yang, S. (1995). Relationships between regional Indian summer monsoon rainfall and Eurasian snow cover. *Advances in Atmospheric Sciences*, *12*(2), 143–150. <https://doi.org/10.1007/bf02656828>
- Pattnayak, K. C., Panda, S. K., & Dash, S. K. (2013). Comparative study of regional rainfall characteristics simulated by RegCM3 and recorded by IMD. *Global and Planetary Change*, *106*, 111–122. <https://doi.org/10.1016/j.gloplacha.2013.03.006>
- Rajeevan, M., & Bhat, J. (2009). A high resolution daily gridded rainfall dataset (1971–2005) for mesoscale meteorological studies. *Current Science*, *96*(4), 558–562.
- Rajeevan, M., Bhat, J., Kale, J. D., & Lal, B. (2005). Development of a high resolution daily gridded rainfall data for the Indian region. *Met. Monogr. No. 22/2005*.
- Randall, D. A., Cess, R. D., Blanchet, J. P., Chalita, S., Colman, R., Dazlich, D. A., et al. (1994). Analysis of snow feedbacks in 14 general circulation models. *Journal of Geophysical Research*, *99*(D10), 20757–20771. <https://doi.org/10.1029/94jd01633>
- Reitter, S., Fröhlich, K., Seifert, A., Crewell, S., & Mech, M. (2011). Evaluation of ice and snow content in the global numerical weather prediction model GME with CloudSat. *Geoscientific Model Development*, *4*(3), 579–589. <https://doi.org/10.5194/gmd-4-579-2011>
- Reynolds, R. W., Rayner, N. A., Smith, T. M., Stokes, D. C., & Wang, W. (2002). An improved in situ and satellite SST analysis for climate. *Journal of Climate*, *15*(13), 1609–1625. [https://doi.org/10.1175/1520-0442\(2002\)015<1609:Aiisas>2.0.Co;2](https://doi.org/10.1175/1520-0442(2002)015<1609:Aiisas>2.0.Co;2)
- Sankar-Rao, M., Lau, K. M., & Yang, S. (1996). On the relationship between Eurasian snow cover and the Asian summer monsoon. *International Journal of Climatology*, *16*(6), 605–616. [https://doi.org/10.1002/\(sici\)1097-0088\(199606\)16:6<605::Aid-joc41>3.0.Co;2-p](https://doi.org/10.1002/(sici)1097-0088(199606)16:6<605::Aid-joc41>3.0.Co;2-p)
- Seol, K.-H., & Hong, S.-Y. (2009). Relationship between the Tibetan snow in spring and the East Asian summer monsoon in 2003: A global and regional modeling study. *Journal of Climate*, *22*(8), 2095–2110. <https://doi.org/10.1175/2008jcli2496.1>
- Shekhar, M. S., & Dash, S. K. (2005). Effect of Tibetan spring snow on the Indian summer monsoon circulation and associated rainfall. *Current Science*, *88*(11), 1840–1844.
- Shepard, D. (1968). A two-dimensional interpolation function for irregularly-spaced data. *Proceedings of the 1968 ACM National Conference, New York, 27-29 August 1968*, 517–524.
- Shukla, J. (1975). Effect of Arabian Sea-surface temperature anomaly on Indian summer monsoon: A numerical experiment with the GFDL model. *Journal of the Atmospheric Sciences*, *32*(3), 503–511. [https://doi.org/10.1175/1520-0469\(1975\)032<0503:Eoasst>2.0.Co;2](https://doi.org/10.1175/1520-0469(1975)032<0503:Eoasst>2.0.Co;2)
- Taylor, K. E. (2001). Summarizing multiple aspects of model performance in a single diagram. *Journal of Geophysical Research*, *106*(D7), 7183–7192. <https://doi.org/10.1029/2000jd900719>
- Tiwari, P. R., Kar, S. C., Mohanty, U. C., Dey, S., Sinha, P., Raju, P. V. S., & Shekhar, M. S. (2016). On the dynamical downscaling and bias correction of seasonal-scale winter precipitation predictions over North India. *Quarterly Journal of the Royal Meteorological Society*, *142*(699), 2398–2410. <https://doi.org/10.1002/qj.2832>
- Vernekar, A. D., Zhou, J., & Shukla, J. (1995). The effect of Eurasian snow cover on the Indian monsoon. *Journal of Climate*, *8*(2), 248–266. [https://doi.org/10.1175/1520-0442\(1995\)008<0248:Teoesc>2.0.Co;2](https://doi.org/10.1175/1520-0442(1995)008<0248:Teoesc>2.0.Co;2)
- Yang, S. (1996). Enso-snow-monsoon associations and seasonal-interannual predictions. *International Journal of Climatology*, *16*(2), 125–134. [https://doi.org/10.1002/\(sici\)1097-0088\(199602\)16:2<125::Aid-joc999>3.0.Co;2-v](https://doi.org/10.1002/(sici)1097-0088(199602)16:2<125::Aid-joc999>3.0.Co;2-v)
- Yang, S., & Xu, L. (1994). Linkage between Eurasian winter snow cover and regional Chinese summer rainfall. *International Journal of Climatology*, *14*(7), 739–750. <https://doi.org/10.1002/joc.3370140704>
- Yihui, D., & Chan, J. C. L. (2005). The East Asian summer monsoon: An overview. *Meteorology and Atmospheric Physics*, *89*(1–4), 117–142. <https://doi.org/10.1007/s00703-005-0125-z>
- Yim, S.-Y., Jhun, J.-G., Lu, R., & Wang, B. (2010). Two distinct patterns of spring Eurasian snow cover anomaly and their impacts on the East Asian summer monsoon. *Journal of Geophysical Research*, *115*, D22113. <https://doi.org/10.1029/2010jd013996>